Supernova Remnants in the Very–high–energy Gamma-ray Domain: the Role of the Cherenkov Telescope Array

M. Santander – University of Alabama

et al.

Deposited 07/03/2019

Supernova remnants in the very–high–energy gamma-ray domain: the role of the Cherenkov telescope array

P. Cristofari,[1]$\star$ S. Gabici,[2] T. B. Humensky,[3] M. Santander,[4] R. Terrier,[2] E. Parizot[2] and S. Casanova[5,6]

[1]*Columbia University, 10027 New York, USA*

[2]*APC, AstroParticule et Cosmologie, Université Paris Diderot, CNRS/IN2P3, CEA/Irfu, Observatoire de Paris, Sorbonne Paris Cité, F-75205 Paris Cedex 13, France*

[3]*Physics Department, Columbia University, 10027 New York, USA*

[4]*Barnard College, Columbia University, 10027 New York, USA*

[5]*Max Planck Institute for Nuclear Physics, D-69117 Heidelberg, Germany*

[6]*Institute for Nuclear Physics, PL-31-342 Krakow, Poland*

ABSTRACT

Supernova remnants are often presented as the most probable sources of Galactic cosmic rays. This idea is supported by the accumulation of evidence that particle acceleration is happening at supernova remnant shocks. Observations in the TeV range have especially contributed to increase the understanding of the mechanisms, but many aspects of the particle acceleration at supernova remnant shocks are still debated. The Cherenkov telescope array is expected to lead to the detection of many new supernova remnants in the TeV and multi-TeV range. In addition to the individual study of each, the study of these objects as a population can help constrain the parameters describing the acceleration of particles and increase our understanding of the mechanisms involved.

Key words: cosmic rays – ISM: supernova remnants – gamma-rays: ISM.

1 INTRODUCTION

Galactic cosmic rays (CRs) are relativistic particles (mainly protons) that fill the entire Galaxy and reach the Earth as an isotropic flux of particles. They are believed to be accelerated at supernova remnant (SNR) shocks via diffusive shock acceleration (e.g. Drury 1983; Bell 2013). This idea is very popular but still needs to be conclusively proven. In order to be the sources of CRs, SNRs must convert ≈ 10 per cent of the supernova explosion energy into relativistic particles, with a spectrum somewhat steeper than $\propto E^{-2}$. Moreover, SNRs must be able to accelerate protons up to the energy of the CR 'knee', located at a particle energy in the range ≈ 1–4×10^{15} eV as suggested from experimental results (Antoni et al. 2005; Bartoli et al. 2015). Finally, the observed chemical composition and the high degree of isotropy of CRs have to be explained as well (see e.g. Hillas 2005; Drury 2012, for reviews).

The success of the SNR paradigm for the origin of CRs resides in the fact that, within this framework, all the above mentioned conditions can be satisfied reasonably well. Recent studies of non-linear diffusive shock acceleration seem to indicate that SNRs can indeed accelerate CRs with roughly the required efficiency, energy spectrum and chemical composition (see e.g. Ptuskin, Zirakashvili &

Seo 2010). As a result of the acceleration of CRs, the magnetic field is expected to be strongly amplified at SNR shocks, up to levels that would allow the acceleration of protons up to the energy of the knee (Bell 2004). This scenario is supported by the fact that magnetic field strengths in the range from hundreds of microGauss to few milliGauss have been inferred from X-ray observations of a number of SNRs (see e.g. Vink 2012, for a review). The high level of isotropy of the arrival direction of CRs at Earth can also be reproduced under certain assumptions on the CR propagation in the Galaxy (Ptuskin et al. 2006; Blasi & Amato 2012). Recently, fine structures have been discovered in the CR spectrum (Adriani et al. 2011; Yoon et al. 2011) that impose additional constraints on the CR acceleration mechanism at SNR shocks (see e.g. Ptuskin, Zirakashvili & Seo 2013).

One of the most promising ways to prove or falsify the scenario described above is to search for the radiation produced by CRs accelerated at SNR shocks. Unambiguous evidence for the acceleration of particles at SNR shocks comes from the observations of individual SNRs in the radio, X-ray and gamma-ray energy domains (see Helder et al. 2012, for a review). Synchrotron emission has been detected from many SNRs in both the radio (e.g. Dubner 2002) and the X-ray bands (e.g. Vink 2012), and this tells us that SNRs can accelerate electrons at least up to the multi-TeV energy range (e.g. Koyama et al. 1995). On the other hand, the gamma-ray emission detected from SNRs can be interpreted either as the result of

hadronic interactions of accelerated protons with the ambient gas or as inverse Compton scattering of electrons on photons of the cosmic microwave background (e.g. Aharonian et al. 2008). Thus, in general it is hard to draw firm conclusions about the acceleration of CR protons from gamma-ray observations only. Recently, conclusive evidence has been obtained for the hadronic nature of the gamma-ray emission detected by *Fermi* and *AGILE* from several older SNRs interacting with molecular clouds (Giuliani et al. 2011; Ackermann et al. 2013; Jogler & Funk 2016), demonstrating that such objects are capable of accelerating CR protons in the GeV energy domain.

The detection of a handful of young (i.e. age up to a few thousand years) SNRs in TeV gamma-rays (Rieger, de Õna Wilhelmi & Aharonian 2013) was long sought and considered a crucial test for the SNR hypothesis for the origin of CRs (Drury, Aharonian & Völk 1994; Naito & Takahara 1994). However, as explained above, such detections do not constitute a final proof for the SNR hypothesis because it is hard to discriminate between gamma-rays produced in hadronic processes or as the result of inverse Compton scattering of electrons off soft ambient photons. Hence, the need for further tests to clarify in an unambiguous way whether SNRs are the sources of Galactic CRs.

In Cristofari et al. (2013, hereafter C13), we proposed a novel test for the SNR hypothesis based on the study of Galactic SNRs as a population. To do so, we performed Monte Carlo simulations to estimate the number of SNRs that one would expect to detect with Cherenkov telescopes of current generation, under the assumption that SNRs indeed are the main sources of Galactic CRs. We then compared our results with the number of actual detections of SNRs within the survey of the Galactic plane performed by the H.E.S.S. collaboration (see e.g. Gast et al. 2012). The agreement found between our predictions and data brings further support to the SNR hypothesis. Moreover, physical constraints to the SNR scenario could be extracted. Most notably, we found that if the SNR hypothesis is correct then the spectrum of accelerated particles at SNR shocks must be steeper than $\approx E^{-2}$ and harder than $\approx E^{-4}$, because an E^{-2} spectrum would result in a number of detections of SNRs much larger than the actual one, and E^{-5} would result in too few detections. Additional constraints include the fact that a significant fraction (roughly $\approx$60 per cent or more, according to model parameters) of the SNRs detected in the H.E.S.S. survey are expected to be characterized by hadronic emission, and the finding that thermonuclear supernovae (type Ia) are expected to account for a large fraction ($\approx 60 - 80$ per cent) of the detections. For a more detailed discussion of these findings we refer the reader to C13.

The results summarized above indicate that the approach we proposed in C13 is powerful, despite the fact that only very few SNRs have been firmly identified within the H.E.S.S. survey of the Galactic plane. With time, new SNR shells (Gottschall et al. 2016) are being detected, and the increased statistics can be confronted with our results to test more accurately and constrain even further the SNR scenario. These larger statistics are expected to be brought by instruments of the next generation such as the Cherenkov telescope array (CTA).

Thus, the main objective of this paper is to evaluate the impact that next-generation instruments such as CTA, operating in the TeV and multi-TeV domain, will have on these studies. After reviewing briefly our method in Section 2, we will make predictions on the number of SNRs detectable by future gamma-ray telescopes. These predictions will be based on the assumption that SNRs are the main sources of CRs. The consistency between our previous results published in C13 and the data currently available from the H.E.S.S.

Galactic plane survey (GPS; Gottschall et al. 2016) argues for the robustness of the predictions presented in this paper. In Section 3 we will consider the case of the GPS of the CTA, whose sensitivity in the TeV energy range is expected to be significantly improved compared to the current Cherenkov telescopes (Hinton et al. 2013). We describe how Monte Carlo simulations confronted with future observations of CTA shall help constrain the parameters involved in the acceleration of Very–high–energy (VHE) particles at SNR shocks, and thus provide a better understanding of the origin of Galactic cosmic rays.

2 COSMIC–RAY ACCELERATION AND GAMMA–RAY PRODUCTION IN GALACTIC SUPERNOVA REMNANTS

In this Section, we briefly describe the Monte Carlo approach used to simulate the time and position of explosion of supernovae within the Galaxy. This procedure is then coupled with a model which describes the acceleration of particles at SNRs and the related production of gamma rays. In this way, the number of SNRs detectable by a given gamma-ray instrument can be computed. This approach was presented in C13, where a detailed description of the model can be found.

2.1 Time and spatial distribution of supernovae in the Galaxy

The time of explosion of all Galactic supernovae is simulated assuming that the supernovae explosion rate is constant in time and equal to $\nu_{\rm SN} = 3$/century (see e.g. Li et al. 2011, and references therein). In fact, this value is quite uncertain within the range extending from about one to a few supernova explosions per century. However, as discussed in C13, results are quite insensitive to the actual choice of this parameter, if the value of the total CR luminosity of the Galaxy is fixed. A type is assigned to each supernova. Four types of supernova are considered: Ia, IIP, Ib/c and IIb. For each, typical values are assumed for the total explosion energy $\mathcal{E}$, the mass of the ejecta $M_{\rm ej}$, the mass-loss rate $\dot{M}$ and the velocity of the wind $u_{\rm w}$ (see e.g. Ptuskin et al. 2010).

Once the time of the explosion and the type of a supernova is drawn, a location within the Galaxy is assigned. The description proposed by Case & Bhattacharya (1998) has been widely used in the literature, but was criticized by Green (2015). Here the distribution of core-collapse supernovae is taken following the description of Faucher-Giguère & Kaspi (2006), assuming that SNRs in the Galaxy follows the radial distribution of pulsars, as presented by Yusifov & Küçük (2004); Lorimer (2004). The surface density at the galactocentric radius r is

$$\rho(r) = A \left(\frac{r + {\rm R}_\odot}{{\rm R}_\odot + R_1} \right)^a \exp \left[-b \left(\frac{r - {\rm R}_\odot}{{\rm R}_\odot + R_1} \right) \right] \quad (1)$$

where ${\rm R}_\odot = 8.5$ kpc is the Sun's galactocentric distance, $R_1 = 0.55$ kpc, $a = 1.64$ and $b = 4.01$ are model parameters taken from Lorimer (2004), and A is a normalization constant determined by imposing a total supernova rate in the Galaxy equal to $\nu_{\rm SN} = 3$/century. Four spiral arms are considered, with each arm following a logarithmic spiral shape. The centroids of the arms are described analytically by equations of the form (Faucher-Giguère & Kaspi 2006):

$$\theta(r) = k\ln(r/r_0) + \theta_0 \quad (2)$$

where r is the galactocentric distance and θ is the polar angle. The parameters k, r_0 and θ_0 are listed in Table 1.

Table 1. Spiral arms parameters from Faucher-Giguère & Kaspi ([2006](#)) to be used in equation (2).

	Name	k (rad)	r_0 (kpc)	θ_0 (rad)
1	Norma	4.25	3.48	1.57
2	Carina–Sagitarius	4.25	3.48	4.71
3	Perseus	4.89	4.90	4.09
4	Crux–Scutum	4.89	4.90	0.95

The spiral structure is realized by drawing first a galactocentric distance r_{raw} from equation (1) and then by choosing randomly an arm. The polar angle θ_{raw} is then determined so that the supernova lies in the centroid of the arm. The actual position of the supernova is finally computed by applying a correction r_{corr} to the galactocentric distance drawn from a normal distribution centred at zero with standard deviation $0.07\,r_{raw}$. To avoid artificial features near the Galactic centre, the distribution is blurred by applying a correction to θ_{raw} also, of magnitude $\theta_{corr}\exp(-0.35r_{raw}\mathrm{kpc})$, where θ_{corr} is randomly chosen in the interval $[0, 2\pi]$ rad.

The spatial distribution of thermonuclear supernovae (type Ia) cannot be traced by the distribution of pulsars, since their progenitors are old stars of relatively low mass. We adopted here the radial distribution of supernovae type Ia plotted in Fig. 10 of Prantzos et al. ([2011](#)), which has been derived from the studies by Scannapieco & Bildsten ([2005](#)). From estimation of the thermonuclear SN rate in the Galaxy (Scannapieco & Bildsten [2005](#)), Prantzos et al. ([2011](#)) have parametrized the SNIa radial profile in the Galaxy. In our work, we consider this parametrized profile and in the inner regions of the Galaxy where the Prantzos description is incomplete (0–2 kpc) we assume a flat distribution normalized using the relative SN rates given by Manucci, Della Valle & Panagia ([2006](#)).

The altitude of the SNRs above (or below) the Galactic plane is determined by assuming that the vertical distribution of the SNRs follows that of the gas (Nakanishi & Sofue [2003](#), [2006](#)). We use the vertical distribution of molecular hydrogen for core-collapse supernovae, and the vertical distribution of atomic Hydrogen for thermonuclear supernovae. This implies that the distribution of thermonuclear supernovae extends up to a height above the disc, which is significantly larger than that of core-collapse supernovae. In the absence of complete knowledge of the spatial distribution of supernovae of a given type, this assumption accounts for the fact that core-collapse supernovae are expected to explode in dense star-forming regions, while thermonuclear ones can also be found in low density regions.

2.2 Evolution of SNRs

The four considered types of progenitors can be divided into two sub-types: thermonuclear supernovae (type Ia) and core-collapse supernovae (all other types), for which the dynamical evolution of the SNR shock is described by different expressions. To determine the time evolution of the SNR shock radius and velocity, we rely on the approach described in Ptuskin & Zirakashvili ([2003](#), [2005](#)), where the CR contribution to the pressure behind the SNR shock is assumed to be significant.

In the case of a thermonuclear supernova, the time evolution of the shock radius R_{sh} and the shock velocity u_{sh} in the ejecta dominated phase are described by self-similar expressions (Chevalier [1982](#); Ptuskin & Zirakashvili [2005](#)). The SNR evolution during the adiabatic phase is computed using the expression given in Truelove & McKee ([1999](#)); Ptuskin & Zirakashvili ([2005](#)). We

follow the SNR evolution until the shock enters the radiative phase, typical after a few 10^4 years (Cioffi, McKee & Bertshinger [1988](#)). In the case of a core-collapse supernova, the shock propagates in the wind-blown bubble generated by the wind of the progenitor star. Ptuskin & Zirakashvili ([2005](#)) suggests to model the wind blown bubble as two regions: a dense red-supergiant wind and a tenuous hot bubble which has been inflated by the wind of the massive progenitor star in main sequence (Weaver et al. [1977](#); Longair [2011](#)). A more detailed description of the environment around core-collapse supernovae can be found in C13. A description of the evolution of the SNR shock during the ejecta dominated phase and the adiabatic phase in this structured interstellar medium is given in Chevalier ([1982](#)); Ptuskin & Zirakashvili ([2005](#)). In the adiabatic phase, the SNR shock evolution can be obtained by adopting the thin-shell approximation (e.g. Ostriker & McKee [1995](#); Bisnovatyi–Kogan & Silich [1995](#)).

Finally, a crucial parameter is the density of the ambient medium, which we derived from the surveys of atomic and molecular hydrogen presented in Nakanishi & Sofue ([2003](#), [2006](#)). Typical values of the ambient density are found in the range $\approx 10^{-5} - 10\ \mathrm{cm}^{-3}$.

2.3 Particle acceleration and gamma emission at SNR shocks

The gamma-ray emission related to the acceleration of particles from a given SNR shell is computed following the method adopted in C13. The contributions to the gamma-ray emission of both nuclei and electrons accelerated at the SNR shocks, through neutral-pion decay and inverse Compton scattering, respectively, are taken into account. The acceleration of particles at the shock is assumed to follow a power-law spectrum $f(R_{sh}, p, t) = A(t)p^{-\alpha}$ where α is regarded in the following as a free parameter. In order to reproduce the slope of the CR spectrum at Earth, studies have suggested that values for alpha should be in the range $\alpha = 4.4 - 4.1$ (e.g. Ptuskin & Zirakashvili [2005](#); Zirakasjvili & Ptuskin [2008a](#); Caprioli, Amato & Blasi [2010](#); Ohira, Murase & Yamazaki [2010](#); Gabici [2011](#); Caprioli [2012](#)) coupled with studies of the propagation of CRs in the Galaxy (see e.g. Strong, Moskalenko & Ptuskin [2007](#), and references therein). By equating the CR pressure at the shock to a fraction $\xi_{CR} \approx 0.1$ of the shock ram pressure, an expression for the normalization $A(t)$ of the CR spectrum can be obtained.

The maximum energy of the accelerated particles is determined by assuming that particles escape the acceleration site once their diffusion length equates a fraction ζ of the shock radius. Several studies suggest $\zeta \approx 0.05 - 0.1$ (e.g. Zirakashvili & Ptuskin [2008b](#), and references therein), and we here take $\zeta = 0.1$ as a reference value.

At the shock, the particle diffusion coefficient depends on the structure and strength of the magnetic field. A high efficiency of the CR acceleration is expected along with a strongly amplified magnetic field and a reduced diffusion coefficient with respect to the typical values found in the interstellar medium. Several mechanisms have been proposed to explain the magnetic field amplification, such as the CR current driven instability (Bell [2004](#)) or the resonant streaming instability (Lagage & Cesarsky [1983](#)) or the Drury instability (Drury & Downes [2012](#)). In the following, we will work under the assumption that in the presence of efficient magnetic field amplification, CR obey Bohm diffusion in the amplified field. The expressions adopted for the magnetic field downstream of the shock B_{down} and for the diffusion coefficient are detailed in C13. Assuming that a fraction $\xi_B = 3.5$ per cent of the ram pressure is converted into magnetic energy, we get $B_{down} \propto (u_{sh}/v_d)$, where v_d is treated as a parameter scaling as $v_d \propto \xi_B^{-1/2}$. Other works have

proposed different descriptions of the evolution of magnetic field at the shock. From X-ray observations, it was for example proposed to describe $B_{down} \propto (u_{sh}/v_d)^{3/2}$ (Bell 2004; Vink 2008; Bykov et al. 2014), with a fraction ξ_B increased within a factor of 2, thus decreasing v_d. In this description, the amplified magnetic field can reach higher values, but for a shorter time (see e.g. Vink 2012, and references therein). Adopting such a description does not affect substantially the results presented in this paper.

Electrons are accelerated at the shock at the same rate as protons. Their spectrum is, however, different, because they suffer synchrotron and inverse Compton losses. At low energies, losses can be neglected, so the acceleration of electrons and protons proceeds similarly: the same spectral shape is thus expected for both species, and a parameter K_{ep} is introduced to describe the ratio between the electron and proton spectra. Indications of values in the range $\approx 10^{-4}$–10^{-2} have been obtained from spectral fits of individual SNRs (see e.g. Ellison et al. 2010; Morlino & Caprioli 2012). For smaller values ($K_{ep} \approx 10^{-5}$ or less), the gamma-ray emission from electrons becomes negligible in comparison to the emission due to pion decay C13. For this reason, in the following we will consider the range $10^{-5} - 10^{-2}$. After being accelerated, the electrons are advected downstream of the shock where they lose energy, mainly through synchrotron radiation.

The magnetic field inside the shell B_{shell} is expected to be significantly smaller than B_{down} if the magnetic field is damped while it is advected downstream of the shock (see e.g. Pohl, Yan & Lazarian 2005; Atoyan & Dermer 2012). In the following we use $B_{shell} = 20\ \mu G$, and we refer the reader to C13 for a more extended discussion of this issue. Because the energy loss time decreases with particle energy, an energy E_{break}^e exists above which the loss time is shorter than the SNR age. Above such energy, the electron spectrum is shaped by radiative losses and steepens by one power in energy with respect to the injection spectrum (see for example Morlino & Caprioli 2012, and references therein). The maximum energy of the electrons E_{max}^e accelerated at a shock can then be obtained by equating the acceleration rate at the shock to the synchrotron energy loss time.

The description of the acceleration of particles inside a SNR can finally be derived by solving a transport equation:

$$\frac{\partial f}{\partial t} + u\nabla f - \nabla D\nabla f - \frac{p}{3}\nabla u \frac{\partial f}{\partial p} = 0 \qquad (3)$$

where D is the momentum-dependent diffusion coefficient for CRs and p the momentum of particles. To describe the structure of the interior of the SNR, we follow the approach of (Ptuskin & Zirakashvili 2003, 2005). Inside the SNR, the structure can be determined by assuming that the velocity is a linear function of the radius and by solving the gas continuity equation (see e.g. Ostriker & McKee 1995). Assuming a CR efficiency in the range 0.05–0.1, we adopt a compatible compression factor $\sigma = 4$. Working under the assumption of such a CR efficiency ensures the validity of the self-similar solutions proposed by Ostriker & McKee (1995). The effect of the plasma thermal conduction in the interior of the SNR (see e.g. Shelton et al. 1999) are not taken into account, but are not expected to be dominant, as our results depend mainly on the evolution of the shock radius and velocity and not on the details of the internal structure.

The reader can refer to C13 for more details. We can therefore finally compute the gamma-ray luminosity from a given SNR. This is done by calculating the hadronic component from proton–proton interactions, following the approach of Kelner, Aharonian & Bugayov (2006), and multiplying results by a factor of 1.8 to take

Table 2. Values of the parameters adopted to compute the curves in Fig. 1, Fig. 2, Fig. 3 and Table 3. α is the slope of the spectrum of CRs accelerated at the shock, and K_{ep} is the electron-to-proton ratio.

Model	α	K_{ep}
M1	4.1	10^{-2}
M2	4.4	10^{-2}
M3	4.4	10^{-5}

into account the nuclei heavier than hydrogen present in the CRs and in the ambient gas (Mori 2009). The leptonic component from inverse Compton scattering of accelerated electrons on the cosmic microwave background is then added (Blumenthal & Gould 1970).

2.4 Comparison with available TeV data: the H.E.S.S. survey of the Galactic plane

In a previous work (Cristofari et al. 2013), a Monte Carlo procedure analogous to the one presented in this article was used to provide a novel test of the SNR paradigm for CR origin. In particular, comparisons with the H.E.S.S. data from the GPS available at the time were used to confront our predictions. The choice of the values of two free parameters was shown to impact dramatically our results, namely, the spectral slope of the particles accelerated at the SNR shock α, and the electron-to-proton ratio K_{ep}. Plausible ranges for these values are $\alpha = 4.1$–4.4 and $K_{ep} = 10^{-5}$–10^{-2} (see Cristofari et al. 2013 for a discussion). Here and in the following we consider three scenarios, labelled M1, M2, M3, and characterized by the values of α and K_{ep} listed in Table 2. Clearly, the scenario M1 (M3) would result in the largest (lowest) number of expected detections of SNRs.

To our knowledge, the most updated results on the H.E.S.S. GPS have been presented in Donath (2016). To date, 78 very-high-energy gamma-ray sources have been detected in the GPS. 31 of them have been firmly identified with known astrophysical objects, while the rest still remain unidentified, or only tentatively identified. Amongst the 31 firm identifications, 8 are SNRs and 8 are composite SNR sources (i.e. it is not clear whether the emission is produced by the SNR or by the associated pulsar wind nebula). Thus, a fraction between 1/4 and 1/2 of the firmly identified sources are SNRs. If this fraction is representative of the entire sample of GPS sources then one might estimate that 20 to 40 out of the 78 GPS sources might be SNRs. Therefore, the most conservative (generous) estimate of the number of SNRs detected in the H.E.S.S. GPS is of $\lesssim 10$ (few tens).

Using the procedure presented in the previous Sections, we computed the number of expected detections of SNRs in the H.E.S.S. GPS, which within the portion of the Galactic disc defined by the coordinate ranges $60° < l < 260°$, $|b| < 2°.5$ is characterized by a roughly uniform sensitivity equal to 1.5 per cent of the Crab flux above 1 TeV. For the two extreme scenarios M1 and M3 we predict 36^{+7}_{-6} and 3.2^{+2}_{-2} detections of SNRs, respectively, compatible with the range inferred from observations.

3 DETECTION OF SNR SHELLS WITH CTA

The Monte Carlo procedure described above is used to simulate the typical population of SNRs expected to be accessible to the CTA. In the following, all results presented have been obtained by averaging
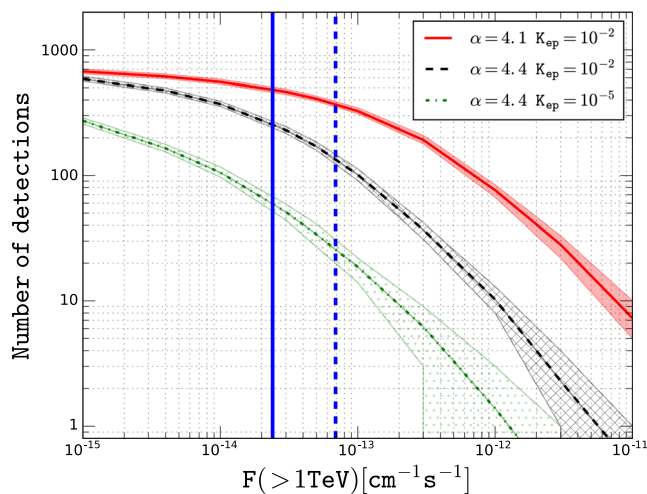
Figure 1. SNRs in the entire Galaxy with integral gamma-ray flux above F(>1 TeV). The red (solid) curve corresponds to model M1, the black (dashed) line corresponds to M2 and the green (dot–dashed) line to M3. In each case the +/– standard deviation is shown. The blue solid and dot–dashed vertical lines correspond to a sensitivity of 1 mCrab and 3 mCrab, respectively.

Figure 2. SNRs in the entire Galaxy with integral gamma-ray flux above F(>10 TeV). Curves as described in caption of Fig. 1. The blue solid and dot–dashed vertical lines correspond to a sensitivity of 10 mCrab and 30 mCrab, respectively.

1000 Monte Carlo realizations of the Galaxy. In fact, a few hundred realizations of the Galaxy are sufficient to produce the results of this article, we take 1000 as a round number.

One of the main scientific goals of the CTA will be to survey areas of the sky to search for faint VHE gamma-ray sources. Most of the currently known VHE sources are located in the Galactic plane. Although the final performance of the array will depend on the exact number of telescopes deployed, it has been shown that CTA could be able to carry out a survey of the entire Galactic plane, directed towards the study of the region $|l| < 60°$, $|b| < 2°$, in ≈1/4 of the available observation time per year, with a uniform sensitivity down to ≈3 mCrab above 1 TeV (Dubus et al. 2013). This corresponds to a flux of ≈6.9×10^{14} cm^{-2} s^{-1}. The details of this hypothetical GPS are still a matter of discussion, but we can consider these values as a reference.

We start by computing the number of SNRs in the Galaxy with integral gamma-ray flux above a given value F(>E). Results are shown in Figs 1 and 2 for F(>1 TeV) and F(>10 TeV), respectively, for the three scenarios M1, M2 and M3 described above and summarized in Table 2.

The blue vertical lines correspond to the typical point-source sensitivity achieved by CTA (impact of extension is discussed below), namely ≈1 mCrab above 1 TeV and ≈10 mCrab above 10 TeV (Dubus et al. 2013). Fig. 1 shows that, for photons of energies above 1 TeV, the models M1, M2 and M3 lead to an average number of SNRs potentially detectable by CTA in a pointed observation of 430, 220 and 48, respectively. At 10 TeV, these numbers are 120, 28 and 5.2. This suggests that under certain circumstances CTA might detect a non-negligible fraction of the whole SNR population in the Galaxy, which can be estimated from the SN rate and a typical maximum age of SNRs of ≈10^5 year, thus ≈3×10^3 potential SNRs. Many SNRs enter the radiative phase younger, suggesting an even larger fraction of young SNRs should be detected. This might constitute the transition between a case-by-case study of gamma-ray bright SNRs to a real population study.

The number of potentially detectable SNRs above 10 TeV is found between several tens or very few objects depending on the parameters adopted. This will have a crucial importance for the
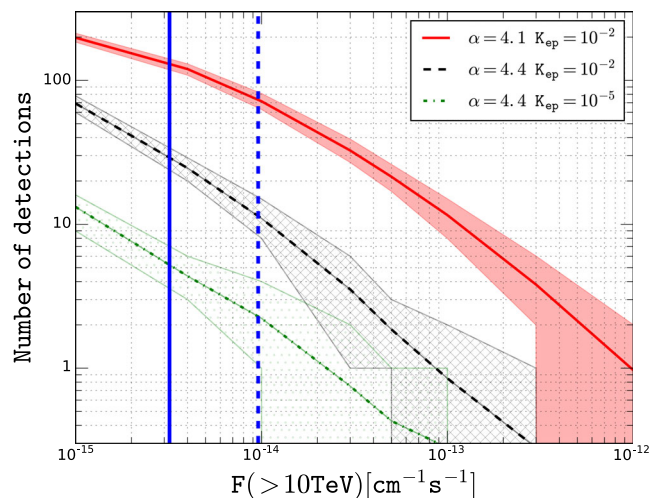
search for PeVatrons (SNRs accelerating PeV particles; see e.g. Gabici, Gaggero & Zandanel 2016, and reference therein).

The numbers in Figs 1 and 2 can be seen as an optimistic and ideal situation, and thus are upper limits for the numbers of detections. This is because several effects can be expected to reduce the number of detections. First of all, it has been described that the sensitivities considered above (represented by the vertical blue lines) will not be achieved in the entire GPS, but only for pointed observations, thus leading to a decrease in the numbers of detections. Secondly, the source extension has not been taken into account. This effect can usually be estimated by degrading the sensitivity of the instrument linearly by the source apparent size when it is larger than the point spread function (PSF) of the instrument (Dubus et al. 2013).

Another effect which will be important is source confusion. The angular extension of the SNRs, the unknown level of the diffusion emission and the high numbers of the sources leading to overlapping between sources may be a significant issue for identification. This effect is expected to be especially relevant in the inner regions of the Galaxy and for the fainter objects (Hewitt & Lemoine-Goumard 2015). According to the latest gamma-ray surveys, the most numerous Galactic sources are pulsar wind nebulae (PWNe) and the overlapping of sources is expected (Donath 2016).

We propose to estimate the effect of the overlapping by the following method. Let us consider overlaps between SNRs and PWNe. The effect of the diffuse emission is not taken into account, since rough extrapolation to the TeV of the diffuse emission measured in the GeV range (Ackermann et al. 2012) suggests that the detection of SNRs will be significantly affected for sources with apparent size of the order of a few 0.°1. For each realization of the time and location of supernovae in the Galaxy that we simulate (as described in Section 2), we simulate the locations and sizes of PWNe in the region of interest, the inner part of the GPS of CTA ($|l| < 60°$, $|b| < 2°$) and we count the number of overlaps between the simulated PWNe and simulated SNRs. The simulation of the PWNe is done as follows: Dubus et al. (2013) estimated that about 300 to 600 PWNe should be detectable depending on the final performances of the telescope. Following the Galactic source distribution model of Renaud & CTA consortium (2011), the number of sources per square degree along each line of sight within $|l| < 60°$, $|b| < 2°$ can

be estimated. First order (i.e. neglecting the local variations at the spiral arm tangents), the resulting Galactic distribution of PWNe is well fitted with a two-dimensional Gaussian at the Galactic centre position with a standard deviation of $\approx 40°$ and $\approx 0°.5$ in Galactic longitude l and latitude b, respectively, and a maximum value in the Galactic centre region of $\approx 4(N_{\mathrm{PWNe}}/500)$ sources per square degree (where N_{PWNe} is the total number of PWNe in the region of interest). In this case, CTA could detect up to ≈ 200 sources in the central regions of the Galaxy $|l| < 30°$, $|b| < 0°.5$ and ≈ 500 sources in the region $|l| < 60°$, $|b| < 2°$. The population of PWNe is expected to be middle aged so that their extension reaches scales of the order of $\approx 0°.1 - 0°.3$ at a few kpc. We study the impact of the average size of the PWNe on the number of confused SNRs (overlaps between SNRs and PWNe, divided by the number of SNRs). For an average size of $0°.1$, the fraction of confused SNRs is negligible even considering 600 PWNe. For an average PWNe size reaching $0°.3$, the fraction of confused SNRs is of ≈ 0.1 and ≈ 0.2 in the cases 300 and 600 PWNe, therefore significantly affecting the detected SNRs. In this study, we also take into account the source confusion due to the superposition of SNRs with other SNRs. We estimate this effect in the case where it is expected to be the most relevant (Model M1), which is the case where the number of detection is the largest. We found that the fraction of SNR–SNR superposition is leading to a confusion fraction smaller than ≈ 0.02. The confusion is therefore expected to be dominated by the superposition with PWNe. In addition, during the H.E.S.S. survey, the number of young SNRs detected was found roughly equal the number of mixed-morphology SNRs, from which the gamma emission is ambiguously due to the shell or the PWN (Donath 2016). This suggests a loss in useful detection of a factor ≈ 2. In the case of CTA, this factor could be reduced, given the improved angular resolution compared to H.E.S.S., but will affect the detected population, favouring smaller (i.e. more distant, younger) sources.

Other very-high-energy gamma-ray sources such as stellar clusters or star forming regions are not taken into account in this work. The confusion with these sources could be estimated in an analogous way, by simulating the number and apparent sizes of these regions, and counting the number of overlappings. By extrapolating the results of the H.E.S.S. GPS, one can argue that the confusion due to these regions is expected to be smaller than the one due to the PWNe population.

As an example of these effects and how they can affect the population of SNRs detected during the GPS, we represent in Fig. 3 the number of SNRs with integral fluxes above F(>1 TeV) in the case of model M1, which is the model leading to the largest number of detections in our study. The red (solid) line corresponds to the case of M1, considering the entire Galaxy, which is the situation described by the solid (red) line of Fig. 1. Taking into account the extension of sources (black dashed line), the number of detections is reduced by a factor of $\approx 1.4 - 1.8$ for sensitivity in 1–3 mCrab. At a sensitivity of 3 mCrab, the number of potentially detectable SNRs drops from ≈ 370 to ≈ 200. The effect becomes negligible for fluxes around $\approx 10^{-15}$ cm^{-1} s^{-2}. We continue by adding the effect (green dot–dashed line) of reducing the survey to a portion of the Galactic plane $|l| < 60°$, $|b| < 2°$, leading to a reduction of roughly factor of $\approx 1.7 - 1.9$ compared to the previous case. At a level of 3 mCrab, the number of potentially detectable SNRs from ≈ 200 to ≈ 120. Finally, the effects of source confusion are added (magenta pointed line). At the level of the sensitivity of CTA, the detection is affected by a factor of ≈ 1.2, which corresponds at 3 mCrab, to a number of ≈ 100 SNRs. We remark that at a level of 10^{-11} cm^{-2} s^{-1}, taking into account the reduced survey, the source

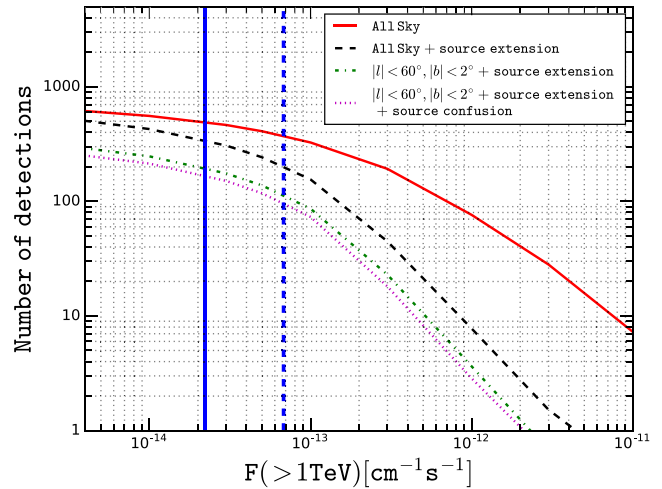**Figure 3.** SNRs with integral gamma-ray flux above F(>1 TeV) in the case of model M1. The red (solid) curve corresponds to the entire Galaxy, the black (dashed) line corresponds to the entire Galaxy and takes into account the effect of the extension of sources. The green (dot–dashed) line corresponds to the inner part of the Galaxy ($|l| < 60°$, $|b| < 2°$) and takes into account the effect of the extension of sources. The magenta (pointed) line corresponds to the same situation as the previous one, but adding the effect of source confusion described in Section 3. The blue solid and dot–dashed vertical lines correspond to a sensitivity of 1 mCrab and 3 mCrab, respectively.

extension and the source confusion, the mean number of detection is $0.2^{+2}_{-0.2}$. In this region, one SNR, RXJ 1713.7–3946 (H. E. S. S. Collaboration et al. 2016), has been detected with such flux. Our results are therefore still compatible with this observation, but illustrate that the computing of the different confusion and extension effects is a first order approximation.

These numbers illustrate how the different effects presented above can be taken into account in our model to simulate the situation corresponding to the performed GPS survey of CTA.

Two strategies have been proposed for the GPS of CTA. A survey of the entire Galactic Plane, where the sensitivity above 1 TeV is typically expected to be ≈ 3 mCrab, and an extensive deeper survey in the central region ($|l| < 60°$, $|b| < 2°$), where the sensitivity could reach the order of ≈ 1 mCrab. We consider these two possible strategies and provide the typical description of the obtained population, considering the three models described previously. Our results are presented in Table 3. In this example, the extension of the sources has been taken into account. The integral fluxes have been degraded linearly by a factor of $\vartheta_s/\vartheta_{\mathrm{PSF}}$, where ϑ_s is the apparent size of the source and $\vartheta_{\mathrm{PSF}} \approx 0°.05$ is the angular resolution of CTA (see e.g. Aharonian et al. 2008, 1997; Carraminana et al. 2008). Naturally, as we go from model M1 to M3, thus from hard to steep spectra and from high-to-low values of the electron-to-proton ratio, the average number of detection of sources decreases. The number of detections can already be compared to the known SNR shells, in the whole Galaxy or in the region of interest. The known number of shells detected in gamma rays in the entire Galaxy is $\gtrsim 13$ (see e.g. Horan & Wakely 2008, describing the TeVCat), although one has to be careful because this number does not account for the circumstances of discovery of these shells, which might have been detected because of their interactions with other objects or extensive targeted observations. This number can be compared with the number of potential detection for Model M3, 8, suggesting indeed that the parameters of M3 are in tension with observation. This is consistent with the

Table 3. Characteristics of the simulated SNR population detected in the GPS of CTA for the different models listed in Table 2. The source extension has been taken into account by degrading the integral fluxes by a factor of $\vartheta_s/\vartheta_{PSF}$, where ϑ_s is the source apparent size and $\vartheta_{PSF} \approx 0°.05$ is the angular resolution of CTA. The *full GPS* and *inner GPS* survey correspond to a sensitivity at 1 TeV of 3 mCrab and 1 mCrab, respectively.

Survey:	Full GPS			Inner GPS		
Model:	M1	M2	M3	M1	M2	M3
Median number of detections:	200	21	7	190	46	18
Median distance (kpc):	8.5	4.5	5.1	10	8.1	7.2
Median age (kyr):	5.0	1.7	0.61	6.7	4.1	4.4
Median apparent size (°)[a]:	0.21	0.20	0.06	0.18	0.20	0.09
Fraction of point sources:	0.17	0.26	0.48	0.15	0.24	0.39
Fraction of hadronic sources:	0.3	0.4	1	0.3	0.4	1

Note. [a]Extended sources only (i.e. size larger than $0°.05$).

fact that several of the observed Galactic SNRs are thought to have their gamma-ray emission dominated by leptonic mechanisms, and therefore a model accounting only for hadronic sources does not seem to agree with observations (Aharonian 2013). From Table 3 we remark that the increased sensitivity in the inner part of the GPS results logically in the detection of more distant and older SNRs. The fraction of point-like sources varies in the different models and observation strategies in the range of 15 per cent – 50 per cent. The models leading to the greater number of detections accounting for the detection of the most extended sources.

The simulated populations of SNRs can be compared to the ones obtained for simulations of the H.E.S.S. GPS. M1 and M2 correspond respectively to model M6 and M5 in Cristofari et al. (2013). We remark that the median distances of the detected SNRs in the CTA GPS simulations in the different models are larger by a factor of $\approx 1.3 - 1.6$, naturally illustrating that the improved sensitivity helps to detect SNRs located further away. In the case of the inner GPS of CTA, the sensitivity above 1 TeV is typically improved by a factor of ≈ 5 compared to H.E.S.S. GPS (from 15 mCrab to 3 mCrab), and for surveys of comparable extension ($|l| < 40°$, $|b| < 3°$ in the former H.E.S.S. GPS, and $|l| < 60°$, $|b| < 2°$ for the inner CTA GPS). If we consider, as an approximation, SNRs to be uniformly distributed in a flat disc, the improvement in sensitivity would lead to SNRs visible up to a distance $\approx 5^{1/2}$. In our case the improvement in the mean distance is found in the range $\approx 1.3 - 1.6$, accounting for the fact that SNRs are not uniformly distributed, and that the survey regions are not exactly equivalent.

The median ages are found larger by a factor of ≈ 1.5, accounting for the detection of older SNRs. The improved sensitivity of CTA leads to a greater number of potentially detectable SNRs and thus the possibility to detect fainter and older objects. At the level of 1 mCrab and in the hypothetical most optimistic case (M1), about $N \approx 500$ SNRs are potentially detectable. If we consider a rate of ν_{SN} 3 SN/century and that these SNRs are uniformly aged, the median age of the population is $\frac{1}{2} \times (N/\nu_{SN}) \approx 8$ kyr. This is without taking into account the source extension and the source confusion described above. Both of these effects select less extended and thus younger SNRs, so that the median age found for M1 is ≈ 5 kyr, as presented in Table 3.

The median size of the resolved sources is comparable to the one found in the H.E.S.S. GPS study and we found that the fraction of resolved sources is a factor of ≈ 2 greater in the CTA GPS. This effect can be explained by the improved angular resolution of CTA, here typically $\approx 0°.05$ at 1 TeV, compared to $\approx 0°.1$ for H.E.S.S. Finally the fraction of hadronic, defined as the contribution from hadronic interactions to the gamma-ray luminosity relative to the total gamma-ray luminosity at 1 TeV, is a factor of ≈ 2 smaller than

in the H.E.S.S. study. This suggests that the improved performance of CTA will lead to a greater number of SNRs with gamma-ray emission dominated by leptonic mechanisms.

A discussion of the influence of several parameters used in this model on our results, such as the rate of Galactic supernova explosion, the structure of the magnetic field or the maximum energy of accelerated particles at the shock can be found in C13. We remark that adopting other realistic descriptions for these parameters tend to decrease the numbers of expected detections, highlighting the fact that results presented in this Section should be seen as upper limits. The most influential parameter in our study appears to be p_{max}. Adopting a different more pessimistic (but still plausible) description of p_{max} leads to numbers of potentially detectable SNRs reduced by a factor of less than $\lesssim 2$.

4 CONCLUSIONS

This paper presents estimates of the SNR population that CTA can expect to detect in the TeV domain. The population study of SNRs that we presented, based on Monte Carlo simulation, aims at being confronted with the results of the CTA GPS. This future confrontation will help test again the SNR paradigm for the origin of CRs, and constrain the parameters governing particle acceleration at SNR shocks.

In the presented work, we have assumed that SNRs are the main sources of CRs, and estimated the typical acceleration efficiency per SNR. A Monte Carlo approach was used to simulate the time and explosion of supernovae in the Galaxy, and to estimate the number of SNRs expected to be detected by CTA. This work had been previously tested on the available data in the TeV domain and the authors believe that this approach is therefore relevant in the TeV and multi-TeV domain for CTA. We have presented the typical populations expected for different extreme values of the electron-to-proton ratio K_{ep} and the slope of accelerated particles at SNR shocks α, and found that in the TeV range, these extreme situations lead to significantly different results. The numbers of SNR detections presented for the observation of the entire Galaxy at the level of ≈ 1 mCrab are 200^{+20}_{-20}, 21^{+5}_{-5} and 8^{+3}_{-3} for Model M1, M2 and M3, respectively. These results suggest that a confrontation with the observation of the CTA GPS could directly give powerful insight on the values of the parameters governing particle acceleration. The numbers of SNR detections in the GPS will be a first direct indicator, and an extensive description of the characteristics of the population could provide arguments in favour of a set of parameters. More models could obviously be considered to constrain more finely the acceleration parameters.

Moreover, it is remarkable that SNRs have been historically detected in the radio wavelength range. Green (2009, 2015) reports a catalogue of $\lesssim 300$ SNRs, and our results suggest that CTA alone could detect a number of SNRs of the same order, therefore becoming a very efficient tool for the detection of SNRs.

These models and values that we have chosen to present correspond to an ideal and optimistic description of the particle acceleration at SNR shocks. Several effects presented in Section 3 are expected to affect these results, such as the extension of the sources, a reduction of the GPS, and the problem of the identification of new SNRs as such. We have described in Section 3 how these effects can be quantitively taken into account. It will therefore be crucial to implement them before confronting the actual CTA observations. We also mention that theoretical advances or observation that would lead to a better description of any of the parameters used in our model, could be implemented in our approach.

The work presented in this paper describes a method which could also be used to investigate the performance of other instruments operating in the TeV range and in the multi-TeV range, such as the HAWC observatory (Abeysekara et al. 2016), LHAASO (Liu et al. 2016) or HiSCORE (Tluczykont et al. 2014), therefore providing more tools to improve our understanding of the origin of Galactic cosmic rays. This work will be carried in a forthcoming paper.

In this paper, we have chosen not to discuss the problem of PeVatrons, though it is indeed a crucial question that instruments operating in the TeV and multi-TeV range will help to address. In the SNR hypothesis for the origin of Galactic CRs, it is often implied that the acceleration of particles up to PeV energies has to be provided by SNR shocks. Observations in the multi-TeV range, where efficient gamma-ray production from leptonic interactions is not possible due to the Klein–Nishina cut-off, could help solve this problem, and therefore provide an unequivocal proof that SNRs are PeVatrons. The clear identification of SNR PeVatrons as such has not been provided by current instruments operating in the TeV range, but the new VHE instruments will provide increased chances of detecting such objects. The model presented in this article can be used to investigate the problem of the detection of PeVatrons and will be presented in a forthcoming paper.

ACKNOWLEDGEMENTS

REFERENCES

Abeysekara A. U. et al., 2016, ApJ, 817, 3
Ackermann M. et al., 2012, ApJ, 750, 3
Ackermann M. et al., 2013, Science, 339, 807
Adriani O. et al., 2011, Science, 332, 69
Aharonian F. A., 2013, Astropart. Phys., 43, 71
Aharonian F. A., Hofmann W., Konopelko A. K., Völk H. J., 1997, Astropart. Phys., 6, 369
Aharonian F. A., Buckley J., Kifune T, Sinnis G., 2008, Rep. Prog. Phys., 71, 096901
Antoni T. et al., 2005, Astropart. Phys., 24, 1
Atoyan A., Dermer C. D., 2012, ApJ, 749, L26
Bartoli B. et al., 2015, Phys. Rev. D, 92, 092005
Bell A. R., 2004, MNRAS, 353, 550
Bell A. R., 2013, Astropart. Phys., 43, 56
Bisnovatyi–Kogan G. S., Silich S. A., 1995, Rev. Mod. Phys., 67, 661
Blasi P., Amato E., 2012, JCAP, 01, 010
Blumenthal G. R., Gould R. J., 1970, Rev. Mod. Phys., 42, 237
Bykov A. M., Ellison D. C., Osipov S. M., Vladimirov A. E., 2014, ApJ, 789, 137
Caprioli D., 2012, JCAP, 07, 038
Caprioli D., Amato E., Blasi P., 2010, Astropart. Phys., 33, 160
Carraminana A., Dingus B., Goodman J., Gonzalez M. 2008, AAS/High Energy Astrophysics Division #10, 10, 41.07
Case G. L., Bhattacharya D., 1998, ApJ, 504, 761
Chevalier R. A., 1982, ApJ, 258, 790
Cioffi D. F., McKee C. F., Bertshinger E., 1988, ApJ, 334, 252
Cristofari P., Gabici S., Casanova S., Terrier R., Parizot E., 2013, MNRAS, 424, 2748
CTA Consortium, 2013, Astropart. Phys., 43, 3
Donath A., 2016, TEVPA talk
Drury L. O'C., 1983, Rep. Prog. Phys., 46, 973
Drury L. O'C., 2012, Astropart. Phys., 39, 52
Drury L. O'C., Aharonian F. A., Völk H. J., 1994, A&A, 287, 959
Drury L. O'C., Downes T. P., 2012, MNRAS, 427, 2308
Dubner G., 2002, in Gopal-Krishna Pramesh Rao A., Swarup G., eds, Proc. IAU Symp. 199, The Universe at Low Radio Frequencies. Pune, India, p. 284
Dubus G. et al., 2013, Astropart. Phys., 43, 317
Ellison D. C., Patnaude D. J., Slane P., Raymond J., 2010, ApJ, 712, 287
Faucher-Giguère C.-A., Kaspi V. M., 2006, ApJ, 643, 332
Gabici S., 2011, Mem. Soc. Astron. Ital., 82, 760
Gabici S., Gaggero D., Zandanel F., 2016, preprint (arXiv:1610.07638)
Gast H. et al., 2012, Proc. 32th Int. Cosmic Ray Conf., 7, 158
Giuliani A. et al., 2011, ApJ, 742, L30
Gottschall D. et al., 2016, preprint (arXiv 1612.00261)
Green D. A., 2009, Bull. Astron. Soc. India, 37, 45
Green D. A., 2015, MNRAS, 454, 1517
H. E. S. S. Collaboration, 2016, preprint (arXiv:1609.08671)
Helder E. A., Vink J., Bykov A. M., Ohira Y., Raymond J. C., Terrier R., 2012, Space Sci. Rev., 173, 369
Hewitt J. W., Lemoine-Goumard M., 2015, C. R. Phys., 16, 674
Hillas A. M., 2005, J. Phys. G: Nucl. Part. Phys., 31, R95
Hinton J., Sarkar S., Torres D., Knapp J., 2013, Astropart. Phys., 43, 1
Horan D., Wakely S., 2008, AAS/High Energy Astrophysics Division #10, 10, 41.06
Jogler T., Funk S., 2016, ApJ, 816, 100
Kelner S. R., Aharonian F. A., Bugayov V. V., 2006, Phys. Rev. D, 74, 034018
Koyama K., Petre R., Gotthelf E. V., Hwang U., Matsuura M., Ozaki M., Holt S. S., 1995, Nature, 378, 255
Lagage P. O., Cesarsky C. J., 1983, A&A, 125, 249
Li W., Chornok R., Leaman J., Filippenko A. V., Poznanski D., Wang X., Ganeshalingam M., Mannucci F., 2011, MNRAS, 412, 1473
Liu Y., Cao Z., Chen S. et al., 2016, ApJ, 826, 63
Longair M. S., 2011, High Energy Astrophysics. Cambridge Univ. Press, Cambridge
Lorimer D. R., 2004, in Camilo F., Gaensler B. M., eds, Proc. IAU Symp. 218, Young Neutron Stars and their Environment. Sydney, Australia, p. 105
Manucci F., Della Valle M., Panagia N., 2006, MNRAS, 370, 773
Mori M., 2009, Astropart. Phys., 31, 341
Morlino G., Caprioli D., 2012, A&A, 538, A81
Naito T., Takahara F., 1994, J. Phys. G: Nucl. Part. Phys., 20, 477
Nakanishi H., Sofue Y., 2003, PASJ, 55, 191
Nakanishi H., Sofue Y., 2006, PASJ, 58, 847
Ohira Y., Murase K., Yamazaki R., 2010, A&A, 513, A17
Ostriker J. P., McKee C. F., 1988, Rev. Mod. Phys., 60, 1
Pohl M., Yan H., Lazarian A., 2005, ApJ, 626, L101
Prantzos N. et al., 2011, Rev. Mod. Phys., 83, 1001
Ptuskin V. S., Zirakashvili V. N., 2003, A&A, 403, 1
Ptuskin V. S., Zirakashvili V. N., 2005, A&A, 429, 755

Ptuskin V. S., Jones F. C., Seo E. S., Sina R., 2006, Adv. Space Res., 37, 1909

Ptuskin V., Zirakashvili V., Seo E.-S., 2010, ApJ, 718, 31

Ptuskin V., Zirakashvili V., Seo E. S., 2013, ApJ, 763, 47

Renaud M., CTA consortium, 2011, Mem. Soc. Astron. Ital., 82, 726

Rieger F. M., de Õna Wilhelmi E., Aharonian F. A., 2013, Frontiers Phys., 8, 714

Scannapieco E., Bildsten L., 2005, ApJ, 83, 1001

Shelton R. L., Cox D. P., Maciejewski W., Randall K. S., Tomasz P., Andrew P., Różyczka M., 1999, ApJ, 524, 192

Strong A. W., Moskalenko I. V., Ptuskin V. S., 2007, Ann. Rev. Nucl. Part. Science, 57, 285

Tluczykont M. et al., 2014, Multifrequency Behaviour of High Energy Cosmic Sources. Palermo, Italy, p. 283

Truelove J. K., McKee C. F., 1999, A&AS, 120, 299

Vink J., 2008, ApJ, 689, 231

Vink J., 2012, A&AR, 20, 49

Weaver R., McCray R., Castor J., Shapiro P., Moore R., 1977, ApJ, 218, 377

Yoon Y. S. et al., 2011, ApJ, 728, 122

Yusifov I, Küçük, I, 2004, A&A, 422, 545

Zirakasjvili V. N., Ptuskin V. S., 2008a, AIP Conf. Proc. Vol. 1085, High Energy Gamma-Ray Astronomy. Am. Inst. Phys., New York, p. 336

Zirakashvili V. N., Ptuskin V. S., 2008b, ApJ, 678, 939

This paper has been typeset from a TEX/LATEX file prepared by the author.